Journal of
Mechanics of
Materials and Structures

MICROMECHANICAL ANALYSIS OF UNIDIRECTIONAL COMPOSITES
USING A LEAST-SQUARES-BASED DIFFERENTIAL
QUADRATURE ELEMENT METHOD

Mohammad Bayat and Mohammad Mohammadi Aghdam

msp

MICROMECHANICAL ANALYSIS OF UNIDIRECTIONAL COMPOSITES USING A LEAST-SQUARES-BASED DIFFERENTIAL QUADRATURE ELEMENT METHOD

MOHAMMAD BAYAT AND MOHAMMAD MOHAMMADI AGHDAM

A generalized plane strain micromechanical model is developed to predict the stress and strain fields and overall elastic properties of a unidirectional fiber-reinforced composite subjected to various axial and transverse normal loading conditions using a least-squares-based differential quadrature element method (DQEM). The representative volume element (RVE) of the composite consists of a quarter of the fiber surrounded by matrix to represent the real composite with a repeating square array of fibers. The cubic serendipity shape functions are used to convert the solution domain to a proper rectangular domain and the new versions of the governing equations and boundary conditions are also derived. The fully bonded fiber-matrix interface condition is considered and the displacement continuity and traction reciprocity are imposed on the fiber-matrix interface. Application of DQEM to the problem leads to an overdetermined system of linear equations mainly due to the particular periodic boundary conditions of the RVE. A least-squares differential quadrature element method is used to obtain solutions for the governing partial differential equations of the problem. The numerical results are in excellent agreement with the available analytical and finite element studies. Moreover, the results of this study reveal that the presented model can provide highly accurate results with a very small number of elements and grid points within each element. In addition, the model shows advantages over conventional analytical models for fewer simplifying assumptions related to the geometry of the RVE.

1. Introduction

Effective and proper use of composites relies on how these materials behave under various types of loading. Both numerical [Adams and Doner 1967; Adams 1970; Eischen and Torquato 1993; Nedele and Wisnom 1994; Sun and Vaidya 1996; Aghdam et al. 2000; 2001; Ahmadi and Aghdam 2010] and analytical [Eshelby 1957; Hashin and Rosen 1964; Hill 1965; Uemura et al. 1979; Mikata and Taya 1985; Nairn 1985; Aboudi 1987; 1989; Nimmer 1990; Robertson and Mall 1993; Aghdam and Dezhestan 2005] micromechanical models have been used to predict the elastic, plastic, and thermal properties of composite materials and their responses to different thermal and mechanical loading conditions.

Numerical models include finite difference [Adams and Doner 1967], finite element [Adams 1970; Nedele and Wisnom 1994; Sun and Vaidya 1996; Aghdam et al. 2000; 2001], boundary element [Eischen and Torquato 1993], and, more recently, meshless [Ahmadi and Aghdam 2010] methods. Among the earliest finite element models, one can refer to [Adams 1970], covering the inelastic behavior of composites subjected to transverse normal loading using a plane strain finite element approach. Other studies on the finite element micromechanical modeling of composites for obtaining overall properties include

various simple uniaxial loading conditions such as longitudinal and transverse normal or shear loading [Sun and Vaidya 1996], combined axial shear and thermal loading [Nedele and Wisnom 1994] and off-axis loading of composites [Aghdam et al. 2001], and yielding and collapse behavior of unidirectional (UD) composites [Aghdam et al. 2000]. The boundary element method [Eischen and Torquato 1993] is also used to study the elastic behavior of composite materials.

Various analytical micromechanical models have also been proposed to evaluate the behavior of heterogeneous materials based on constituent properties, volume fractions, and their interactions. Among the first analytical approaches to model composite behavior were the model presented in [Eshelby 1957] and the self-consistent model of [Hill 1965]. Analytical models based on the variational principles of the theory of elasticity [Hashin and Rosen 1964] have also been employed to obtain upper and lower bounds of the overall elastic properties of composite materials. In these models, while the minimum complementary energy method yields the lower bounds, the minimum potential energy principle results in the upper bounds.

There is another class of analytical models in which a small area of the composite is considered as a representative volume element (RVE) of the composite. These types of models can be categorized into various groups based on the simplifying assumptions made about the geometry of the composite. The two major groups are composite cylinder models (CCM) and unit cell models (UCM). The geometry of the RVE in CCM consists of a circular fiber surrounded by a circular matrix [Uemura et al. 1979]. In some cases, more than two concentric cylinders were considered to study the effects of the interface [Nairn 1985] and fiber coating [Mikata and Taya 1985]. In UCM however, the cross section of the RVE includes a rectangular fiber surrounded by several rectangular blocks of matrix. One of the well-known micromechanical models in the category of UCM is the method of cells (MC), which was developed in [Aboudi 1987; 1989]. This model has several advantages compared with other similar models while also being mathematically rigorous. More UCM types of models can be found elsewhere [Nimmer 1990; Robertson and Mall 1993; Aghdam and Dezhestan 2005].

Analytical models normally require more rigorous mathematical procedures [Aboudi 1987; 1989] while normally involving more simplifying assumptions [Aboudi 1987; 1989; Nimmer 1990; Robertson and Mall 1993; Aghdam and Dezhestan 2005]. Furthermore, most analytical models are not able to provide a nonuniform distribution of stress and strain fields within the RVE, though their predictions for overall properties are reasonably accurate. In numerical techniques, however, there are fewer simplifying assumptions, and accuracy depends on the number of elements or grid points. For instance, in order to obtain more accurate results in finite element analysis, the geometry of the RVE should be divided into a few hundred small elements.

In the past decade, the differential quadrature element method (DQEM) has been used to study the behavior of different structural elements [Wang et al. 1996; Wang and Gu 1997; Karami and Malekzadeh 2002; Chen 2003]. However, apart from applications of the differential quadrature (DQ) method in fluid mechanics, all the studies in the literature have been restricted to various 2D elasticity problems of isotropic and laminated plates and shells; the method has not been used in micromechanics of heterogeneous materials. These studies revealed that the method offers a good convergence rate and accuracy with a relatively small number of grid points. However, implementation of boundary conditions is a challenging and time-consuming procedure in DQEM. This is mainly due to the resultant overdetermined system of algebraic equations in most DQEM problems. In order to prevent formation of overdetermined system

of equations after implementation of multiboundary conditions, several approaches have been presented in the literature. For example, some DQ equations at inner nodes can be replaced by the additional boundary conditions. However, it has been found that the accuracy of the results may vary depending on which DQ equations at the inner grids are replaced by the boundary conditions [Zong and Zhang 2009]. Jang et al. [1989] proposed the so-called δ-technique wherein, adjacent to the boundary points of the differential quadrature grid, points are chosen at a small distance $\delta \cong 10^{-5}$ (as a dimensionless value). Then the DQ analog of the two conditions at a boundary are written for the boundary points and their adjacent δ-points. Wang and Bert [1993] introduced an approach where the boundary conditions are formed during formulation of the weighting coefficients for higher-order derivatives. Malik and Bert [1996] tried to employ this approach for all boundary conditions. Wang et al. [1996; Wang and Gu 1997] introduced another method in which multiboundary conditions are imposed by assigning two degrees of freedom to each end point for a fourth-order differential equation. Wu and Liu [2000] proposed a generalized differential quadrature rule, introducing multiple degrees of freedom at boundary points. Recently, Karami and Malekzadeh [2002] proposed a method of applying the multiboundary conditions. In formulations of the weighting coefficients of third and fourth-order derivatives, the second derivatives at the boundary points are viewed as additional independent variables.

Briefly, in order to adjust the number of equations and unknowns, researchers normally eliminate some of the equations [Wang 2001] or add extra unknowns to the problem [Karami and Malekzadeh 2002; Wu and Liu 2000]. However, in this study all of the governing equations and boundary conditions are considered and, therefore, the resultant overdetermined system of equations is solved using a least-squares technique.

In this study, a two-dimensional generalized plane strain micromechanical model is presented to predict the behavior of a UD composite system using DQEM. The geometry of the RVE is divided into three elements, as shown in Figure 1, which are then mapped to a rectangular domain using the cubic serendipity shape functions (see Figure 2). The fully bonded fiber-matrix interface condition is considered and the displacement continuity and traction reciprocity are imposed on the fiber-matrix interface. The new version of the governing partial differential equations of the problem and their boundary and interface conditions are obtained. Application of DQEM to the problem leads to an overdetermined system of linear equations mainly due to the particular periodic boundary conditions of the RVE. A least-squares differential quadrature element method (LSDQEM) is used to obtain solutions for the governing partial differential equations of the problem. The results of this study show excellent agreement with the finite element analysis for various stress and displacement components of a SiC/Ti composite system. The predicted overall properties of the same SiC/Ti system also show excellent agreement with other analytical and finite element analyses.

2. Analysis

2.1. *Geometry of the model.* In a real UD fiber-reinforced composite, the fibers are likely to be arranged in a random array. It is difficult, if not impossible, to model the composite behavior with the real constituent geometry. Apart from some approximate bounds found for a random array of fibers and arbitrary phase geometry using a variational method [Hill 1965], the actual cross section of the composite has to be idealized as a regular array of fibers. In most analytical, finite element, and numerical models,
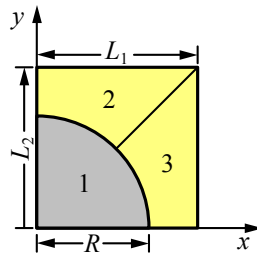
Figure 1. Geometry of the RVE and selected elements.
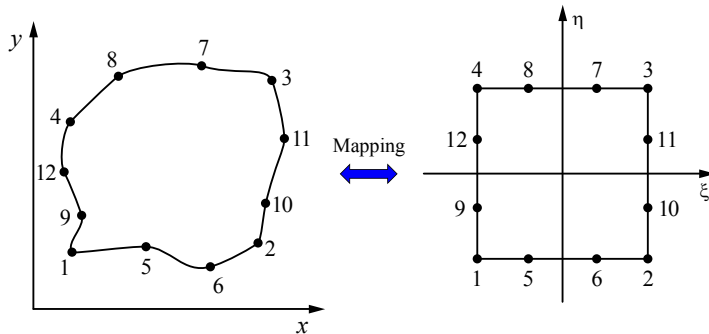
Figure 2. Mapping of the cubic serendipity element from the physical domain (left) to the computational domain (right).

the cross section of the composite is simplified as periodic arrays of fibers, either in a square or hexagonal array packing, as shown in Figure 3. In this study, the fibers are assumed to be arranged in square arrays. The second step is to choose the smallest informative and repeating area of the geometry for the whole cross section as the RVE. It is assumed that all the effective characteristics and global behavior of the composite are similar to those of the RVE. Hence, special care should be taken to select the correct RVE and to apply the correct boundary conditions to model the real loading conditions on the composite. Commonly, a quarter of the fiber and the corresponding matrix, as shown in Figure 1, are sufficient to model various loading conditions.
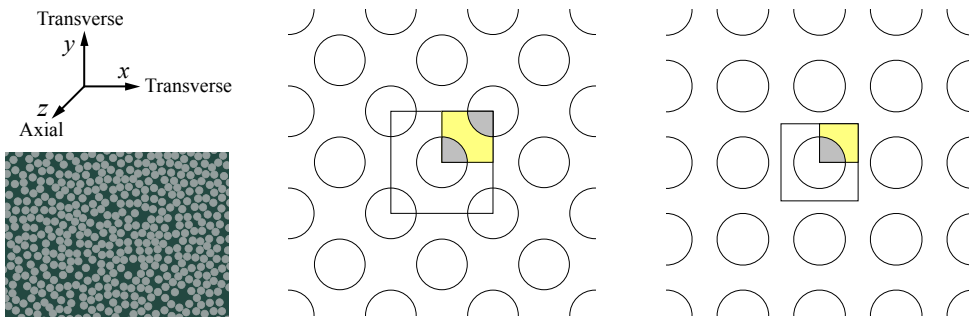
Figure 3. Left: schematic diagram of a real UD composite. Middle: unit cell and RVE of hexagonal array. Right: unit cell and RVE of square array.

2.2. *Governing equations.* Assuming a generalized plane strain condition which can provide more realistic predictions, the displacement fields within the RVE can be considered as

$$u = u(x, y), \quad v = v(x, y), \quad w = \varepsilon_{z0} \cdot z, \tag{1}$$

where u, v, and w are displacements in the x, y, and z directions, respectively, and ε_{z0} is an unknown constant strain in the fiber direction to be determined. Based on the theory of elasticity, the strain-displacement relations within the RVE are

$$\varepsilon_x = u_{,x}, \quad \varepsilon_y = v_{,y}, \quad \varepsilon_z = w_{,z}, \quad \gamma_{xy} = v_{,x} + u_{,y}, \quad \gamma_{xz} = w_{,x} + u_{,z}, \quad \gamma_{yz} = w_{,y} + v_{,z}, \tag{2}$$

in which $(\ )_{,x} \equiv \partial(\ )/\partial x$. The generalized plane strain condition for displacements requires vanishing shear strains $\gamma_{xz} = \gamma_{yz} = 0$ and consequently zero shear stresses $\tau_{xz} = \tau_{yz} = 0$. Furthermore, assuming linear elastic behavior for both constituents, stress-strain relations for each phase of the RVE can be written as

$$\sigma_x = B(u_{,x} + Cv_{,y} + C\varepsilon_{0z}), \qquad \sigma_y = B(Cu_{,x} + v_{,y} + C\varepsilon_{0z}),$$
$$\sigma_z = B(Cu_{,x} + Cv_{,y} + \varepsilon_{0z}), \qquad \tau_{xy} = G(v_{,x} + u_{,y}), \tag{3}$$

where constants B and C are

$$B = \frac{E(1-\nu)}{(1+\nu)(1-2\nu)}, \quad C = \frac{\nu}{1-\nu}, \tag{4}$$

in which E and ν are the elasticity modulus and the Poisson's ratio of the constituents, respectively. Finally, the governing equilibrium equations of the problem in the absence of body forces can be written in terms of displacement components as

$$\alpha u_{,xx} + \beta v_{,xy} + u_{,yy} = 0, \quad \alpha v_{,yy} + \beta u_{,xy} + v_{,xx} = 0, \tag{5}$$

where $\alpha = 2(1-\nu)/(1-2\nu)$ and $\beta = 1/(1-2\nu)$.

2.3. *Mapping the geometry of the RVE.* In this study, a RVE corresponding to a square array of fibers is considered. In order to apply DQEM to solve the governing equations, the RVE is divided into three irregular regions/elements, as shown in Figure 1. Using geometric natural-to-Cartesian mappings, an irregular quadrilateral physical domain (x, y), as shown in Figure 2, can be mapped into a normalized computational domain (ξ, η) based on the following cubic serendipity shape function:

$$x = \sum_{i=1}^{12} N_i(\xi, \eta) \cdot x_i, \quad y = \sum_{i=1}^{12} N_i(\xi, \eta) \cdot y_i \quad (-1 \leq \xi, \eta \leq 1), \tag{6}$$

where $N_i(\xi, \eta)$ is the cubic serendipity shape function defined by

$$N_i(\xi, \eta) = \tfrac{1}{32}(1 + \xi\xi_i)(1 + \eta\eta_i)[9(\xi^2 + \eta^2) - 10], \qquad i = 1, 2, 3, 4,$$
$$N_i(\xi, \eta) = \tfrac{9}{32}(1 - \xi^2)(1 + \eta\eta_i)(1 + 9\xi\xi_i), \qquad\qquad i = 5, 6, 7, 8, \tag{7}$$
$$N_i(\xi, \eta) = \tfrac{9}{32}(1 + \xi\xi_i)(1 - \eta^2)(1 + 9\eta\eta_i), \qquad\qquad i = 9, 10, 11, 12,$$

in which ξ_i and η_i are the coordinates of the node i in the ξ-η domain. In order to obtain the new version of the governing equations in the computational square element, the Jacobian of transformation matrix,

$$[J] = \begin{bmatrix} x_{,\xi} & y_{,\xi} \\ x_{,\eta} & y_{,\eta} \end{bmatrix},$$

is inverted:

$$[J]^{-1} = \begin{bmatrix} \xi_{,x} & \eta_{,x} \\ \xi_{,y} & \eta_{,y} \end{bmatrix} = \frac{1}{|J|} \begin{bmatrix} y_{,\eta} & -y_{,\xi} \\ -x_{,\eta} & x_{,\xi} \end{bmatrix}, \quad |J| = x_{,\xi} y_{,\eta} - x_{,\eta} y_{,\xi}, \tag{8}$$

where $|J|$ is the determinant of the Jacobian matrix. Thus, the transformation of the first-order derivatives is

$$\begin{Bmatrix} u_{,x} \\ u_{,y} \end{Bmatrix} = [J]^{-1} \begin{Bmatrix} u_{,\xi} \\ u_{,\eta} \end{Bmatrix}. \tag{9}$$

To include second-order derivatives, the transformation may be written in matrix form as

$$\begin{Bmatrix} u_{,\xi} \\ u_{,\eta} \\ u_{,\xi\eta} \\ u_{,\xi\xi} \\ u_{,\eta\eta} \end{Bmatrix} = \begin{bmatrix} x_{,\xi} & y_{,\xi} & 0 & 0 & 0 \\ x_{,\eta} & y_{,\eta} & 0 & 0 & 0 \\ x_{,\xi\eta} & y_{,\xi\eta} & x_{,\xi}y_{,\eta}+x_{,\eta}y_{,\xi} & x_{,\xi}x_{,\eta} & y_{,\eta}y_{,\xi} \\ x_{,\xi\xi} & y_{,\xi\xi} & 2x_{,\xi}y_{,\xi} & x_{,\xi}^2 & y_{,\xi}^2 \\ x_{,\eta}^2 & y_{,\eta}^2 & 2x_{,\eta}y_{,\eta} & x_{,\eta}^2 & y_{,\eta}^2 \end{bmatrix} \begin{Bmatrix} u_{,x} \\ u_{,y} \\ u_{,xy} \\ u_{,xx} \\ u_{,yy} \end{Bmatrix}. \tag{10}$$

The inverse transformation can be expressed as explicit functions of (ξ, η), similar to (9). Implementation of the DQ method on the computational square domain is straightforward.

2.4. DQ method. The quadrature rules for a function $\Psi = \Psi(x, y)$ on a rectangular domain ($0 \le x \le a$, $0 \le y \le b$), can be written as follows [Bert and Malik 1996]:

$$\left.\frac{\partial^r \Psi}{\partial x^r}\right|_{x=x_i} = \sum_{k=1}^{N_x} A_{ik}^{(r)} \Psi_{kj}, \quad i = 1, 2, \dots, N_x, \qquad \left.\frac{\partial^s \Psi}{\partial y^s}\right|_{y=y_j} = \sum_{l=1}^{N_y} B_{jl}^{(s)} \Psi_{il}, \quad j = 1, 2, \dots, N_y, \tag{11}$$

$$\int_{x=0}^{a} \Psi(x, y_j)\,dx = \sum_{k=1}^{N_x} C_k \Psi_{kj}, \qquad \int_{y=0}^{b} \Psi(x_i, y)\,dy = \sum_{l=1}^{N_y} C_l \Psi_{il},$$

$$\int_{x=0}^{a}\int_{y=0}^{b} \Psi(x, y)\,dx\,dy = \sum_{k=1}^{N_x} C_k \sum_{l=1}^{N_y} D_l \Psi_{kl}, \qquad \left.\frac{\partial^{(r+s)} \Psi}{\partial x^r \partial y^s}\right|_{x_i,y_j} = \left.\frac{\partial^r}{\partial x^r}\left(\frac{\partial^s \Psi}{\partial y^s}\right)\right|_{x_i,y_j} = \sum_{k=1}^{N_x} A_{ik}^{(r)} \sum_{l=1}^{N_y} B_{jl}^{(s)} \Psi_{kl},$$

where N_x and N_y are the numbers of grid points in the x and y directions, respectively, $\psi_{ij} = \psi(x_i, y_j)$, and $A_{ij}^{(r)}$, $B_{ij}^{(s)}$, C_i, and D_i are weighting coefficients. For example, in order to determine the weighting coefficients $A_{ik}^{(r)}$, the Lagrange interpolation basic functions [Shu and Richards 1992b; Bert et al. 1993] are used as test functions and, therefore, explicit formulas for computing the weighting coefficients of the first-order derivative can be obtained as follows [Shu and Richards 1992a]:

$$A_{ik}^{(1)} = \frac{\prod(x_i)}{(x_i - x_k)\prod(x_k)} \quad \text{for} \quad i, k = 1, 2, \dots, N_x \quad \text{and} \quad k \ne i, \qquad \prod(x_i) = \prod_{v=1, v \ne k}^{N_x} (x_i - x_v). \tag{12}$$

For higher-order derivatives, one can use the following relations iteratively:

$$A_{ik}^{(r)} = r\left[A_{ii}^{(r-1)} A_{ik}^{(1)} - \frac{A_{ik}^{(r-1)}}{x_i - x_k}\right] \quad \text{for } i, k = 1, 2, \ldots, N_x \text{ and } \quad k \neq i, \quad 2 \leq r \leq (N_x - 1),$$

$$A_{ii}^{(r)} = -\sum_{v=1, v\neq i}^{N_x} A_{iv}^{(r)} \quad\quad\quad \text{for } i = 1, 2, \ldots, N_x, \quad 1 \leq r \leq (N_x - 1). \tag{13}$$

The next step is the discretization of the domain to $N_\xi \times N_\eta$ grid points. It is shown [Shu et al. 2001] that one of the best options for obtaining grid points is zeros of the well-known Chebyshev polynomials:

$$\xi_i = -1 + \cos\left[\frac{(i-1)\pi}{N_\xi - 1}\right], \ i = 1, 2, \ldots, N_\xi, \quad\quad \eta_j = -1 + \cos\left[\frac{(j-1)\pi}{N_\eta - 1}\right], \ j = 1, 2, \ldots, N_\eta. \tag{14}$$

In DQEM, the procedure of the DQ method should be repeated for the governing equation within each element. Therefore, the governing equations (5) can be written in the computational domain as

$$(\alpha\xi_{,x}^2 + \xi_{,y}^2)\sum_{k=1}^{N_\xi} A_{ik}^{(2)} u_{kj} + (\alpha\eta_{,x}^2 + \eta_{,y}^2)\sum_{l=1}^{N_\eta} B_{jl}^{(2)} u_{il} + (\alpha\xi_{,xx} + \xi_{,yy})\sum_{k=1}^{N_\xi} A_{ik}^{(1)} u_{kj}$$

$$+ (\alpha\eta_{,xx} + \eta_{,yy})\sum_{l=1}^{N_\eta} B_{jl}^{(1)} u_{il} + (2\alpha\xi_{,x}\eta_{,x} + 2\xi_{,y}\eta_{,y})\sum_{k=1}^{N_\xi} A_{ik}^{(1)}\sum_{l=1}^{N_\eta} B_{jl}^{(1)} u_{kl}$$

$$+ (\beta\xi_{,x}\xi_{,y})\sum_{k=1}^{N_\xi} A_{ik}^{(2)} v_{kj} + (\beta\eta_{,x}\eta_{,y})\sum_{l=1}^{N_\eta} B_{jl}^{(2)} v_{il} + (\beta\xi_{,xy})\sum_{k=1}^{N_\xi} A_{ik}^{(1)} v_{kj}$$

$$+ (\beta\eta_{,xy})\sum_{l=1}^{N_\eta} B_{jl}^{(1)} v_{il} + \beta(\xi_{,x}\eta_{,y} + \xi_{,y}\eta_{,x})\sum_{k=1}^{N_\xi} A_{ik}^{(1)}\sum_{l=1}^{N_\eta} B_{jl}^{(1)} v_{kl} = 0,$$

$$(\xi_{,x}^2 + \alpha\xi_{,y}^2)\sum_{k=1}^{N_\xi} A_{ik}^{(2)} v_{kj} + (\eta_{,x}^2 + \alpha\eta_{,y}^2)\sum_{l=1}^{N_\eta} B_{jl}^{(2)} v_{il} + (\xi_{,xx} + \alpha\xi_{,yy})\sum_{k=1}^{N_\xi} A_{ik}^{(1)} v_{kj}$$

$$+ (\eta_{,xx} + \alpha\eta_{,yy})\sum_{l=1}^{N_\eta} B_{jl}^{(1)} v_{il} + (2\xi_{,x}\eta_{,x} + 2\alpha\xi_{,y}\eta_{,y})\sum_{k=1}^{N_\xi} A_{ik}^{(1)}\sum_{l=1}^{N_\eta} B_{jl}^{(1)} v_{kl}$$

$$+ (\beta\xi_{,x}\xi_{,y})\sum_{k=1}^{N_\xi} A_{ik}^{(2)} u_{kj} + (\beta\eta_{,x}\eta_{,y})\sum_{l=1}^{N_\eta} B_{jl}^{(2)} u_{il} + (\beta\xi_{,xy})\sum_{k=1}^{N_\xi} A_{ik}^{(1)} u_{kj}$$

$$+ (\beta\eta_{,xy})\sum_{l=1}^{N_\eta} B_{jl}^{(1)} u_{il} + \beta(\xi_{,x}\eta_{,y} + \xi_{,y}\eta_{,x})\sum_{k=1}^{N_\xi} A_{ik}^{(1)}\sum_{l=1}^{N_\eta} B_{jl}^{(1)} u_{kl} = 0.$$

2.5. *Compatibility, loading, and boundary conditions.* Assuming a perfectly bonded interface between the fiber and matrix, the following displacement continuity and traction reciprocity conditions should be satisfied at the common nodes of the two adjacent elements:

$$u^a = u^b, \quad v^a = v^b, \quad \sigma_x^a \cdot n_1 + \tau_{xy}^a \cdot n_2 = \sigma_x^b \cdot n_1 + \tau_{xy}^b \cdot n_2, \quad \tau_{xy}^a \cdot n_1 + \sigma_y^a \cdot n_2 = \tau_{xy}^b \cdot n_1 + \sigma_y^b \cdot n_2, \tag{15}$$

where a and b refer to two adjacent elements and $n = (n_1, n_2)$ is unit normal to the interface. Furthermore, appropriate loading and boundary conditions for the normal loading of the RVE in the transverse and axial directions are (Figure 1):

$$
\begin{aligned}
u = \tau_{xy} = 0 &\qquad\qquad\qquad \text{on} \quad x = 0, \\
v = \tau_{xy} = 0 &\qquad\qquad\qquad \text{on} \quad y = 0, \\
u = \text{const.}, \quad \tau_{xy} = 0, \quad \int_0^{L_2} \sigma_x \, dy = \sigma_{x0} L_2 &\qquad \text{on} \quad x = L_1, \\
v = \text{const.}, \quad \tau_{xy} = 0, \quad \int_0^{L_1} \sigma_y \, dx = \sigma_{y0} L_1 &\qquad \text{on} \quad y = L_2, \\
\varepsilon_{z0} = \text{const.}, \quad \int_0^{L_1}\int_0^{L_2} \sigma_z \, dx\, dy = \sigma_{z0} L_1 L_2 &\qquad \text{on the RVE},
\end{aligned}
\tag{16}
$$

in which σ_{x0}, σ_{y0}, and σ_{z0} are the applied macrostress components on the RVE in the x, y, and z directions, respectively. The compatibility conditions at the element interface and the boundary conditions have a dominant influence on the accuracy of the results and, therefore, (15) and (16) should be mapped to the computational domain and discretized carefully.

Application of DQEM to the problem together with the boundary and compatibility conditions leads to an overdetermined system of algebraic linear equations $Ax = b$, that is, A is a rectangular matrix of size $m \times n$, $n < m$. In order to solve the nonsymmetric linear system $Ax = b$, one may use an equivalent system,

$$
A^T A x = A^T b,
\tag{17}
$$

which is symmetric positive definite. This system is known as the system of the normal equations associated with the following least-squares problem:

$$
\text{minimize } \|b - Ax\|_2,
\tag{18}
$$

in which $\|b - Ax\|_2 \equiv (\sum_{i=1}^m [b_i - \sum_{j=1}^n A_{ij} x_j]^2)^{1/2}$. It can be shown that minimizing (18), which is a least-squares solution for the nonsymmetric linear system $Ax = b$, leads to the symmetric system (17); see, for instance, [Saad 2003] for more details.

Finally, it is interesting to note that application of DQEM leads to a compatible overdetermined system of equations, and therefore, the above-mentioned least-squares technique results in accurate predictions.

3. Numerical results and discussion

The procedure explained in the previous sections is used to obtain stress and displacement components within the fiber and matrix of a SiC/Ti metal matrix composite with a 40% fiber volume fraction (FVF). The composite is subjected to normal loading in the axial and transverse directions. Various overall properties of the composite system can also be determined by applying uniaxial loads. The mechanical properties of the constituents of the SiC/Ti system are as follows (see [Aghdam et al. 2000]):

$$
\begin{aligned}
\text{SiC (fiber):} &\quad E = 409 \, \text{GPa} \quad \nu = 0.2 \\
\text{Ti (matrix):} &\quad E = 107 \, \text{GPa} \quad \nu = 0.3
\end{aligned}
$$
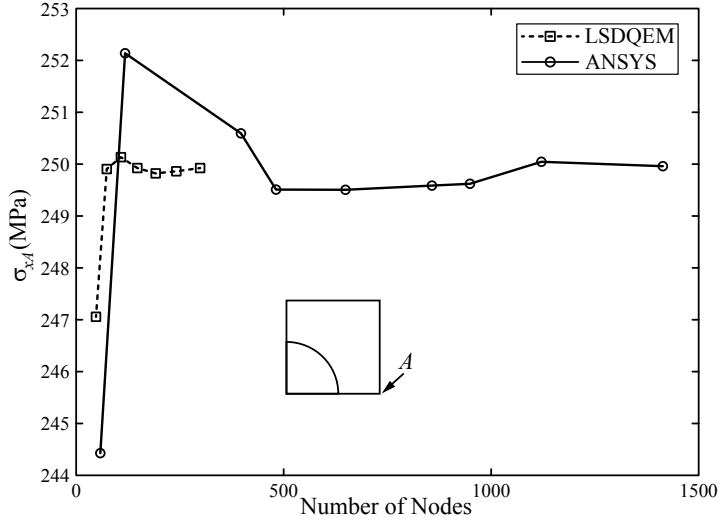
Figure 4. Convergence of transverse normal stress σ_x at point A, with $\varepsilon_{x0} = 0.001$.

3.1. *Convergence study and CPU time.* In this section, the convergence rate and CPU time of the presented method are compared with those of ANSYS and a mesh-free method for two examples. In the first example, a UD SiC/Ti metal matrix composite with a 40% FVF is considered. The RVE is subjected to a uniform strain of $\varepsilon_{x0} = 0.001$ in the x direction on the right-hand side, while all other stress and strain components are zero. Figure 4 represents the convergence of the transverse normal stress σ_x at point A of the RVE. The figure also includes convergence of the same results obtained by the commercial finite element code ANSYS [ANSYS 2008]. The geometry of the RVE in the ANSYS simulation is modeled by two-dimensional generalized plane strain PLANE183 elements with eight nodes. The results suggest that very good convergence can be achieved by using about 100 nodes in LSDQEM while FEM analysis requires more than 1000 nodes for the same level of convergence.

The efficiency of the presented method is examined in another example in which a boron/aluminum metal matrix composite with a 47% FVF is considered. The material properties of the constituents are as follows:

$$\text{Boron (fiber)} \quad E = 379.3 \,\text{GPa} \quad \nu = 0.2$$
$$\text{Aluminum (matrix)} \quad E = \ 68.3 \,\text{GPa} \quad \nu = 0.3$$

The overall transverse Young's modulus of the boron/aluminum composite (E_T^c) is calculated using three different methods including the presented LSDQEM, FEM (ANSYS), and meshless method [Ahmadi and Aghdam 2010]. The CPU times for these methods are tabulated in Table 1. Again, it can be

Method	Number of nodes	CPU time (s)	E_T^c (GPa)
LSDQEM	108	6	143.92
FEM (ANSYS)	1200	~15	143.96
Meshless method [Ahmadi and Aghdam 2010]	350	14.9	144.31

**Table 1.** Comparison of the CPU time for LSDQEM and other methods (FVF $= 0.47$).

seen that the number of nodes and the CPU time for LSDQEM are significantly less than for the other two methods which implies efficiency for the presented method. The predictions of the presented model for the transverse Young's modulus (E_T^c) are also in excellent agreement with the predictions of ANSYS.

3.2. *Stress analysis.*

Transverse normal loading. In this section, the SiC/Ti composite system with a 40% FVF subjected to a transverse strain of $\varepsilon_{x0} = 0.001$ in the x direction is considered. The RVE is assumed to be square, that is, $L_1 = L_2$. In order to examine the validity of the results, another analysis was also carried out using the finite element code ANSYS [ANSYS 2008]. All the predicted stress and displacement components show excellent agreement with the finite element results for the entire domain of the problem. For example, the comparison of the normal stress σ_x is presented in Figure 5. The stresses and displacements within the
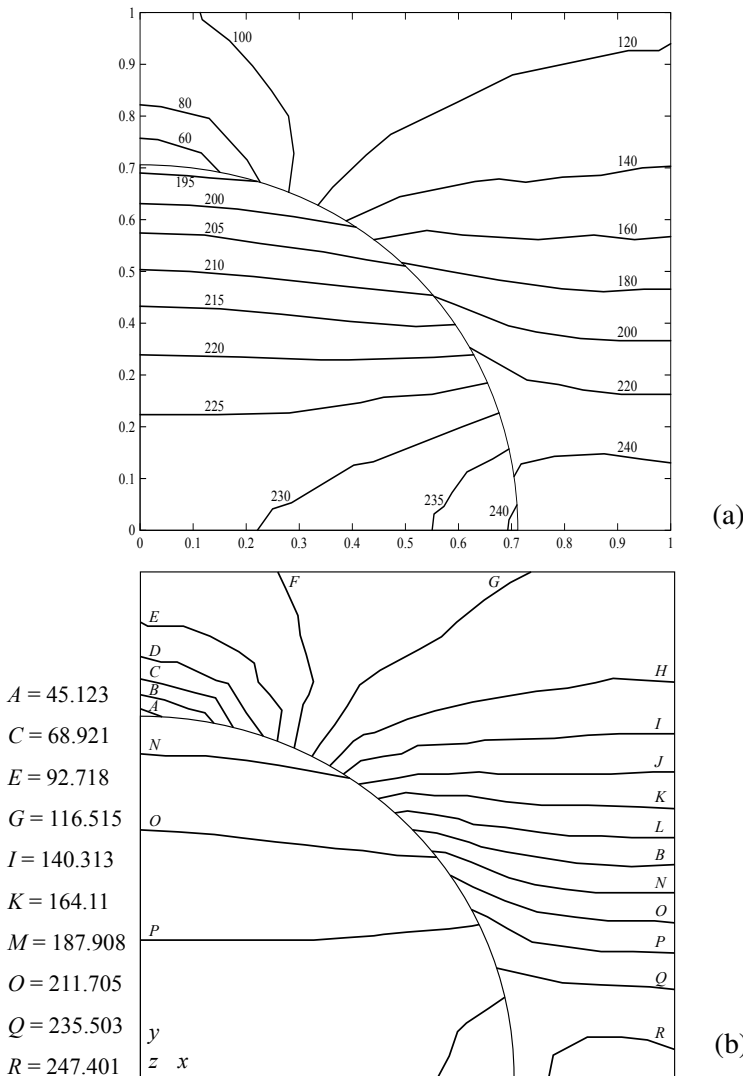
Figure 5. Contours of normal stress σ_x (in MPa) in the RVE of (a) DQEM and (b) ANSYS.
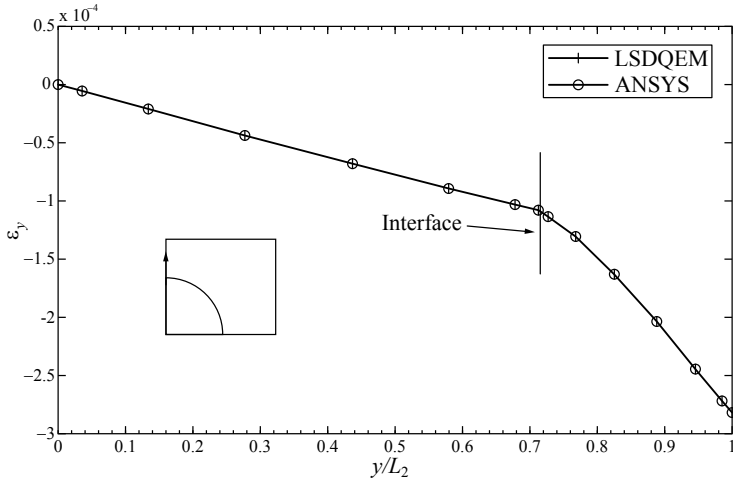
Figure 6. Comparison of ε_y along the y-axis, with $\varepsilon_{x0} = 0.001$.
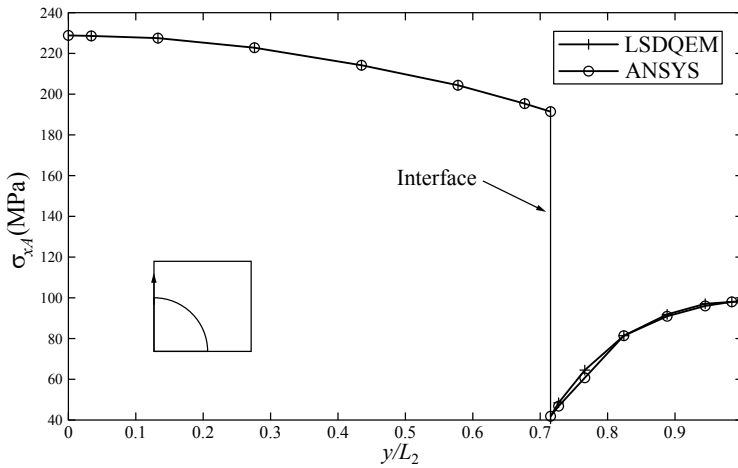
Figure 7. Comparison of normal stress σ_x along the y-axis, with $\varepsilon_{x0} = 0.001$.

RVE are compared with the finite element results in Figures 6–8. As expected, it can be seen in Figures 6–8 that ε_y and σ_y are continuous along the y-axis while σ_x and σ_z are discontinuous at the fiber-matrix interface. Furthermore the SiC/Ti composite is subjected to a uniaxial transverse normal load in the x direction, $\sigma_x = 100$ MPa. The dimensionless stress σ^* is defined as the ratio of the microstress σ to the applied macrostress $\overline{\sigma} = 100$ MPa, that is, $\sigma^* = \sigma/100$. The distribution of the dimensionless normal and effective von Mises σ_e^* stresses on the x and y axes of the RVE are shown in Figures 9 and 10. It is seen that on the x-axis the microstress σ_x^* is greater than the applied macrostress. The coefficient of stress concentration for transverse loading is $\sigma_{x\max}/\sigma_x = 1.4$. As expected, it can also be seen that σ_x along the x-axis (Figure 9) and σ_y along the y-axis (Figure 11) are continuous, while the other stresses are discontinuous at the fiber-matrix interface.

Axial normal stress loading. The uniaxial axial normal load in the z direction, $\sigma_z = 100$ MPa, is applied to a SiC/Ti composite system. The resultant dimensionless normal and effective von Mises σ_e^* stresses
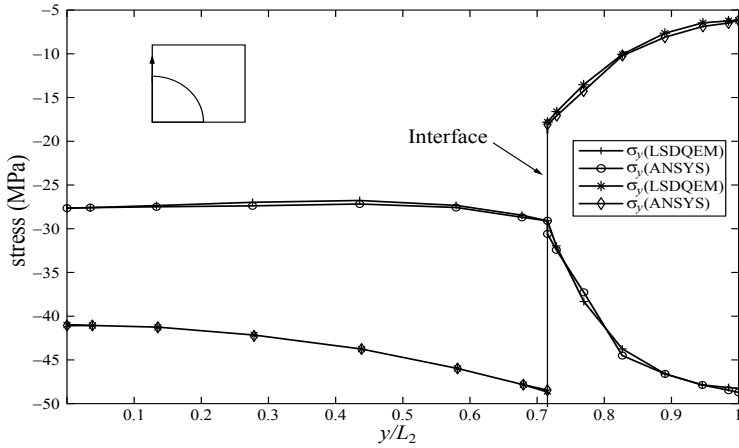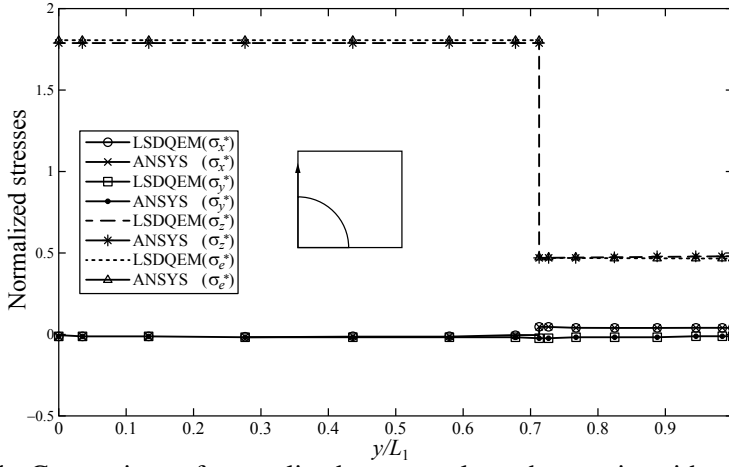
Figure 8. Comparison of normal stresses (σ_y, σ_z) along the y-axis, with $\varepsilon_{x0} = 0.001$.
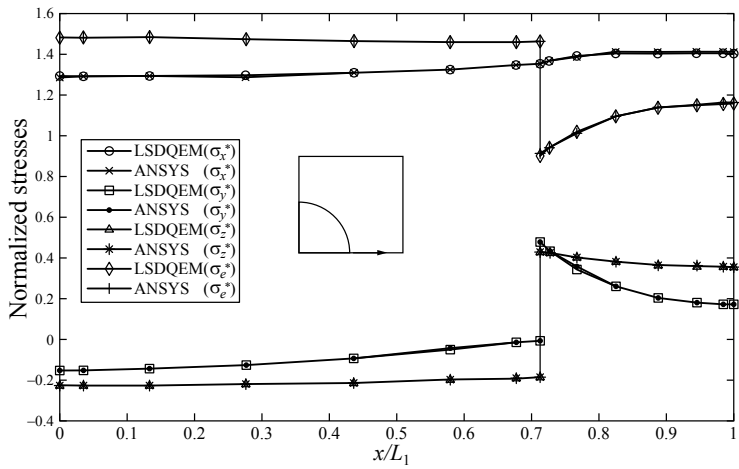
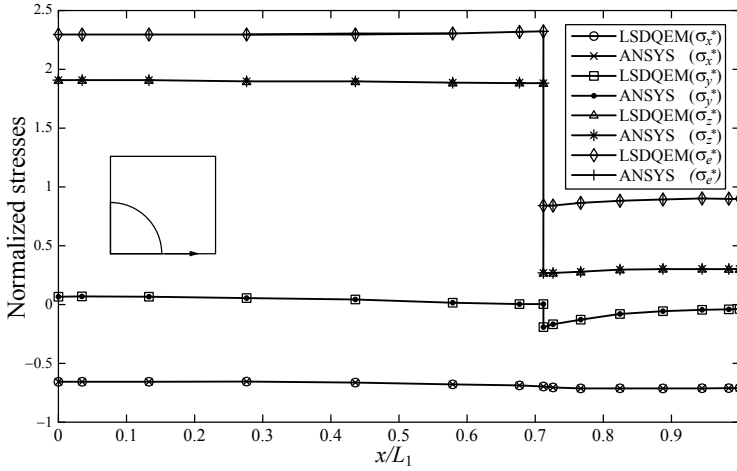**Figure 9.** Comparison of normalized stresses along the x-axis, with $\sigma_x = 100$ MPa.
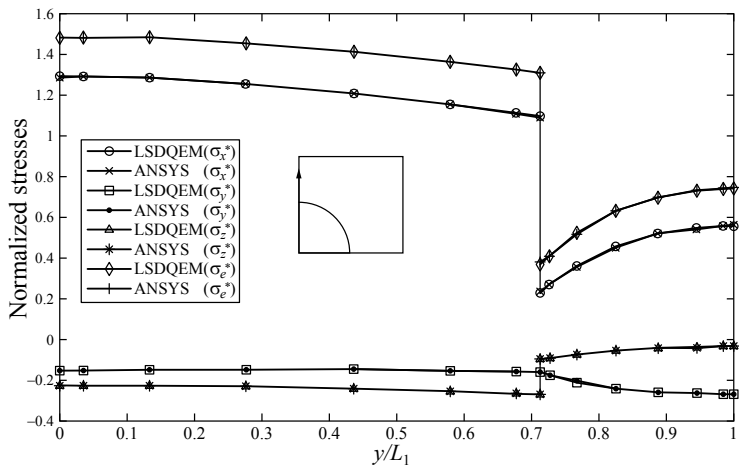
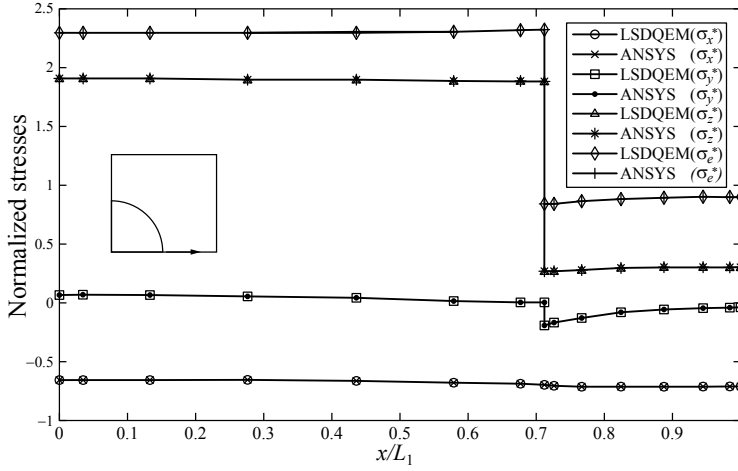**Figure 10.** Comparison of normalized stresses along the y-axis, with $\sigma_x = 100$ MPa.

Figure 11. Comparison of normalized stresses along the y-axis, with $\sigma_z = 100$ MPa.

Figure 12. Comparison of normalized stresses along the x-axis, with $\sigma_x = -50$ MPa, $\sigma_z = 100$ MPa.

on the y-axis of the RVE are shown in Figure 11. It is seen that the microstress σ_z^* within the fiber is greater than the applied macrostress. The coefficient of stress concentration for the axial loading is $\sigma_{z\,\max}/\sigma_z = 1.79$. As expected, σ_z is nearly constant within the fiber and matrix with larger a value in the fiber which results from the generalized plane strain assumption and all other stress components are nearly zero.

Biaxial normal stress loading. In the next example, the SiC/Ti composite system subjected to a biaxial normal stress of $\sigma_x = -50$ MPa, $\sigma_z = 100$ MPa is studied. The dimensionless normal and effective von Mises σ_e^* stresses on the x axis of the RVE are shown in Figure 12. It can be seen that σ_x along the x-axis, Figure 12, is continuous while the other stresses are discontinuous at the fiber-matrix interface. Furthermore σ_z is nearly constant within the fiber and matrix.

Figure 13. Comparison of normalized stresses along the x-axis, with $\sigma_x = -50$ MPa, $\sigma_y = 80$ MPa, $\sigma_z = 100$ MPa.

Triaxial normal stress loading. Finally, the SiC/Ti composite system subjected to a triaxial normal stress of $\sigma_x = -50$ MPa, $\sigma_y = 80$ MPa, $\sigma_z = 100$ MPa is considered. The distribution of the dimensionless stresses on the x-axis of the RVE is shown in Figure 13. All the predicted stress components show excellent agreement with the finite element results.

3.3. *Elastic properties.* In order to obtain the overall mechanical properties of the composite system, the square RVE is analyzed using uniaxial loadings in the transverse and longitudinal directions. For instance, the RVE is subjected to a uniform stress in the x direction (σ_{x0}) while the other stress components (σ_{y0}, σ_{z0}) are zero. Then, the overall strain of the RVE in the x and y directions ($\varepsilon_{x0}, \varepsilon_{y0}$) can be determined. The transverse Young's modulus and Poisson's ratio can be calculated using

$$E_T^c = \sigma_{x0}/\varepsilon_{x0}, \quad \nu_T^c = |\varepsilon_{y0}/\varepsilon_{x0}|, \tag{19}$$

in which the superscript c refers to the overall composite property. A similar procedure can be used to obtain the axial properties of the composite system. Predictions for the overall transverse Young's modulus, E_T^c, of the SiC/Ti are shown in Table 1. It should be noted that three elements with 8×8 grid points are considered in the presented DQEM while more elements are used in the finite element analysis.

Included in Table 2 are also results from finite element analysis [Aghdam et al. 2000] and the method of cells (MC) [Aboudi 1987]. As can be seen in Table 2, all the predictions are in close agreement with each other. It should be noted that due to geometrical restrictions for the square array fiber assumption, the maximum fiber volume fraction (FVF) for both the finite element method and DQEM is 0.785. The predictions for the overall transverse Poisson's ratio, ν_T^c, for the same material are shown in Table 2. Again, excellent agreement can be seen between the DQEM and finite element results while the results of MC shows an overestimate for the entire range of the FVF. The predictions for the overall longitudinal Young's modulus, E_L^c, and Poisson's ratio, ν_L^c, of the SiC/Ti composite system are depicted in Table 2.

FVF	Solution method	E_L^c (GPa)	ν_L^c	E_T^c (GPa)	ν_T^c
20%	LSDQEM	167.63	0.2766	136.66	0.3103
	ANSYS	167.62	0.2766	136.74	0.3099
	FEM	168.80	0.2612	136.91	0.3102
	MC	167.93	0.2637	135.18	0.323
40%	LSDQEM	228.13	0.2550	177.86	0.2820
	ANSYS	228.12	0.2550	177.93	0.2818
	FEM	228.61	0.2252	177.75	0.2822
	MC	227.75	0.2274	169.5	0.3130
60%	LSDQEM	288.56	0.2348	234.46	0.2450
	ANSYS	288.54	0.2348	234.35	0.2455
	FEM	289.30	0.1913	243.23	0.2458
	MC	288.86	0.1929	217.29	0.2885

Table 2. Comparison of the longitudinal (axial) and transverse Young's moduli and Poisson's ratios for various fiber volume fractions (FVF). The FEM values are from [Aghdam et al. 2000] and the method of cells (MC) values from [Aboudi 1987].

The predictions of the MC and finite element analysis are also included in the table. The MC predictions can be obtained by the closed form solutions given in [Aboudi 1987].

4. Concluding remarks

A micromechanical model is developed to predict the behavior of a unidirectional (UD) fiber-reinforced composite subjected to various axial and transverse normal loading conditions using the differential quadrature element method (DQEM). The theory of elasticity is used to derive the governing partial differential equations of the problem. The geometry of the representative volume element (RVE) is then divided into three elements and mapping is used to convert the solution domain to a computational square domain. The new versions of the governing equations and boundary conditions are derived.

The application of DQEM for this problem leads to an overdetermined system of linear equations since the RVE has particular boundary conditions. The least-squares approximation is used to solve the resultant system of equations. It is demonstrated that the least-squares differential quadrature element method (LSDQEM) is a simple and fast approach to imposing the various boundary conditions of the problem. It can be seen that the number of nodes and the CPU time for LSDQEM are significantly less than for the mesh-free method and FEM. Comparison of the predicted results for various stress and displacement components shows excellent agreement with the finite element method. Moreover, results for overall the mechanical properties of the UD composites also show excellent agreement with other published analytical and finite element models. In addition, the model has the advantage over conventional analytical models of making fewer simplifying assumptions on the geometry of the RVE.

References

[Aboudi 1987] J. Aboudi, "Closed form constitutive equations for metal matrix composites", *Int. J. Eng. Sci.* **25**:9 (1987), 1229–1240.

[Aboudi 1989] J. Aboudi, "Micromechanical analysis of composites by the method of cells", *Appl. Mech. Rev.* (*ASME*) **42**:7 (1989), 193–221.

[Adams 1970] D. F. Adams, "Inelastic analysis of a unidirectional composite subjected to transverse normal loading", *J. Compos. Mater.* **4**:3 (1970), 310–328.

[Adams and Doner 1967] D. F. Adams and D. R. Doner, "Transverse normal loading of a unidirectional composite", *J. Compos. Mater.* **1**:2 (1967), 152–164.

[Aghdam and Dezhestan 2005] M. M. Aghdam and A. Dezhestan, "Micromechanics based analysis of randomly distributed fiber reinforced composites using simplified unit cell model", *Compos. Struct.* **71**:3–4 (2005), 327–332.

[Aghdam et al. 2000] M. M. Aghdam, M. J. Pavier, and D. J. Smith, "Finite element micromechanical modelling of yield and collapse behaviour of metal matrix composites", *J. Mech. Phys. Solids* **48**:3 (2000), 499–528.

[Aghdam et al. 2001] M. M. Aghdam, M. J. Pavier, and D. J. Smith, "Micro-mechanics of off-axis loading of metal matrix composites using finite element analysis", *Int. J. Solids Struct.* **38**:22–23 (2001), 3905–3925.

[Ahmadi and Aghdam 2010] I. Ahmadi and M. M. Aghdam, "Micromechanics of fibrous composites subjected to combined shear and thermal loading using a truly meshless method", *Comput. Mech.* **46**:3 (2010), 387–398.

[ANSYS 2008] *ANSYS user's manual*, Version 11.0, Swanson Analysis Systems, Houston, TX, 2008.

[Bert and Malik 1996] C. W. Bert and M. Malik, "Differential quadrature method in computational mechanics: a review", *Appl. Mech. Rev.* (*ASME*) **49**:1 (1996), 1–28.

[Bert et al. 1993] C. W. Bert, X. Wang, and A. G. Striz, "Differential quadrature for static and free vibrational analyses of anisotropic plates", *Int. J. Solids Struct.* **30**:13 (1993), 1737–1744.

[Chen 2003] C.-N. Chen, "DQEM and DQFDM for the analysis of composite two-dimensional elasticity problems", *Compos. Struct.* **59**:1 (2003), 3–13.

[Eischen and Torquato 1993] J. W. Eischen and S. Torquato, "Determining elastic behavior of composites by the boundary element method", *J. Appl. Phys.* **74**:1 (1993), 159–170.

[Eshelby 1957] J. D. Eshelby, "The determination of the elastic field of an ellipsoidal inclusion, and related problems", *Proc. R. Soc. Lond. A* **241**:1226 (1957), 376–396.

[Hashin and Rosen 1964] Z. Hashin and B. W. Rosen, "The elastic moduli of fiber-reinforced materials", *J. Appl. Mech.* (*ASME*) **31**:2 (1964), 223–232.

[Hill 1965] R. Hill, "A self-consistent mechanics of composite materials", *J. Mech. Phys. Solids* **13**:4 (1965), 213–222.

[Jang et al. 1989] S. K. Jang, C. W. Bert, and A. G. Striz, "Application of differential quadrature to static analysis of structural components", *Int. J. Numer. Methods Eng.* **28**:3 (1989), 561–577.

[Karami and Malekzadeh 2002] G. Karami and P. Malekzadeh, "A new differential quadrature methodology for beam analysis and the associated differential quadrature element method", *Comput. Methods Appl. Mech. Eng.* **191**:32 (2002), 3509–3526.

[Malik and Bert 1996] M. Malik and C. W. Bert, "Implementing multiple boundary conditions in the DQ solution of higher-order PDEs: application to free vibration of plates", *Int. J. Numer. Methods Eng.* **39**:7 (1996), 1237–1258.

[Mikata and Taya 1985] Y. Mikata and M. Taya, "Stress field in a coated continuous fiber composite subjected to thermo-mechanical loadings", *J. Compos. Mater.* **19**:6 (1985), 554–578.

[Nairn 1985] J. A. Nairn, "Thermoelastic analysis of residual stresses in unidirectional, high-performance composites", *Polym. Compos.* **6**:2 (1985), 123–130.

[Nedele and Wisnom 1994] M. R. Nedele and M. R. Wisnom, "Finite element micromechanical modelling of a unidirectional composite subjected to axial shear loading", *Composites* **25**:4 (1994), 263–272.

[Nimmer 1990] R. P. Nimmer, "Fiber-matrix interface effects in the presence of thermally induced residual stress", *J. Compos. Technol. Res.* **12**:2 (1990), 65–75.

[Robertson and Mall 1993] D. D. Robertson and S. Mall, "Micromechanical relations for fiber-reinforced composites using the free transverse shear approach", *J. Compos. Technol. Res.* **15**:3 (1993), 181–192.

[Saad 2003] Y. Saad, *Iterative methods for sparse linear systems*, 2nd ed., Chapter 8, pp. 245–259, SIAM, Philadelphia, 2003.

[Shu and Richards 1992a] C. Shu and B. E. Richards, "Application of generalized differential quadrature to solve two dimensional incompressible Navier–Stokes equations", *Int. J. Numer. Methods Fluids* **15**:7 (1992), 791–798.

[Shu and Richards 1992b] C. Shu and B. E. Richards, "Parallel simulation of incompressible viscous flows by generalized differential quadrature", *Comput. Sys. Eng.* **3**:1–4 (1992), 271–281.

[Shu et al. 2001] C. Shu, W. Chen, H. Xue, and H. Du, "Numerical study of grid distribution effect on accuracy of DQ analysis of beams and plates by error estimation of derivative approximation", *Int. J. Numer. Methods Eng.* **51**:2 (2001), 159–179.

[Sun and Vaidya 1996] C. T. Sun and R. S. Vaidya, "Prediction of composite properties from a representative volume element", *Compos. Sci. Technol.* **56**:2 (1996), 171–179.

[Uemura et al. 1979] M. Uemura, H. Iyama, and Y. Yamaguchi, "Thermal residual stresses in filament-wound carbon-fiber-reinforced composites", *J. Therm. Stresses* **2**:3–4 (1979), 393–412.

[Wang 2001] Y. Wang, *Differential quadrature method and differential quadrature element method-theory and practice*, Ph.D. thesis, Nanjing University of Aeronautics and Astronautics, Nanjing, 2001. In Chinese.

[Wang and Bert 1993] X. Wang and C. W. Bert, "A new approach in applying differential quadrature to static and free vibrational analyses of beam and plates", *J. Sound Vib.* **162**:3 (1993), 566–572.

[Wang and Gu 1997] X. Wang and H. Gu, "Static analysis of frame structures by the differential quadrature element method", *Int. J. Numer. Methods Eng.* **40**:4 (1997), 759–772.

[Wang et al. 1996] X. Wang, H. Gu, and B. Liu, "On buckling analysis of beams and frame structures by the differential quadrature element method", pp. 382–385 in *Engineering mechanics: proceedings of the 11th conference* (Fort Lauderdale, FL, 1996), vol. 1, edited by Y. K. Lin and T. C. Su, ASCE, New York, 1996.

[Wu and Liu 2000] T. Y. Wu and G. R. Liu, "Application of generalized differential quadrature rule to sixth-order differential equations", *Commun. Numer. Methods Eng.* **16**:11 (2000), 777–784.

[Zong and Zhang 2009] Z. Zong and Y. Zhang, *Advanced differential quadrature methods*, CRC Press, Boca Raton, FL, 2009.

MOHAMMAD BAYAT: mbayat@aut.ac.ir
Department of Mechanical Engineering, Amirkabir University of Technology, 424 Hafez Avenue, Tehran 15875-4413, Iran

MOHAMMAD MOHAMMADI AGHDAM: aghdam@aut.ac.ir
Department of Mechanical Engineering, Amirkabir University of Technology, 424 Hafez Avenue, Tehran 15875-4413, Iran
http://me.aut.ac.ir/M.Aghdam.htm

JOURNAL OF MECHANICS OF MATERIALS AND STRUCTURES

jomms.net

Founded by Charles R. Steele and Marie-Louise Steele

Cover design: Alex Scorpan   Cover photo: Mando Gomez, www.mandolux.com

See http://jomms.net for submission guidelines.

Journal of Mechanics of Materials and Structures